Journal of Photochemistry & Photobiology, A: Chemistry 404 (2021) 112879

Contents lists available at ScienceDirect

Journal of Photochemistry & Photobiology, A: Chemistry

journal homepage: www.elsevier.com/locate/jphotochem

Electrospun nanofibrous sheet doped with a novel triphenylamine based salicylaldehyde fluorophore for hydrazine vapor detection

Apisit Karawek [a], Pipattra Mayurachayakul [a], Thanapich Santiwat [a], Mongkol Sukwattanasinitt [b], Nakorn Niamnont [a,*]

[a] Organic Synthesis, Electrochemistry & Natural Product Research Unit, Department of Chemistry, Faculty of Science, King Mongkut's University of Technology Thonburi, Bangkok, 10140, Thailand

[b] Organic Synthesis Research Unit, Department of Chemistry, Faculty of Science and Nanotec-CU Center of Excellence on Food and Agriculture, Chulalongkorn University, Bangkok, 10330, Thailand

ARTICLE INFO

Keywords:
Electrospun nanofibrous
Hydrazine
Salicylaldehyde

ABSTRACT

Successful synthesis of a novel triphenylamine based salicylaldehyde fluorophore (compound **1**) was performed via Suzuki cross-coupling reaction. Subsequently, the identification the hydrazine vapor of an electrospun nanofiber sheet combined with compound **1** depending on solid condition was described. Furthermore, cellulose acetate (**CA**) combined with the electrospun nanofiber sheet based on compound **1** was formed by applying the electrospinning technique where the average diameter was 324.6 ± 91.6 nm. The sensing nanofiber sheet exhibited a sensitive and selective reaction to hydrazine vapor with a linear concentration range of 0.2-1 %w/v in aqueous solution according to the analysis of fluorescence images using ImageJ. Moreover, it exhibited the elevated selectivity with hydrazine across 21 convenient interferences. Initial findings revealed the nanofibrous mat's sensitivity and selectivity in terms of the identification of hydrazine via naked-eye detection under backlight 365 nm with fluorescent turn-off mode. Additionally, the generation of compound **1** and the hydrazone product (compound **1-HZ**) was investigated through the use of ^{1}H-NMR titration and HRMS, which affirmed the formation of hydrazine with a proton chemical shift at 7.95 ppm, HRMS of compound **1-HZ** at m/z = 380.1764 [**1-HZ**+H]$^+$). It has been demonstrated that the nanofibrous mat offers a basic and suitable method for detecting water vapour in water environments as well as industrial chemical setting.

1. Introduction

Hydrazine (N_2H_4) is a critical chemical reagent that plays a pivotal role in various fields, including medicines, chemicals used in photography, pigments, textile dyes and materials for reducing the rate of corrosion in a variety of chemical industries [1–2]. Additionally, it is recognised for its use in rocket propulsion due to its increased enthalpy of combustion [3–4]. Despite its different benefits, it is known to be a carcinogen with high toxicity that has the potential to cause significant pollution to the environment along with a risk of damaging health as a result of the processes involved in manufacturing, using, transporting and disposing of the substance [5–6]. It has the potential to cause serious damage to the liver, lungs, kidneys and the nervous system as absorbance of hydrazine can occur easily via the mouth, skin or by being inhaled subsequent to exposure [7–9]. Authorities around the world have placed strict regulations on the amount of hydrazine permissible in potable water, with limits typically being low micromolar levels [10]. Resultantly, it is necessary to develop robust and simple analytical techniques that can detect trace amounts of hydrazine.

A variety of analytical approaches can be implemented for detecting molecules of hydrazine, including chromatography [11], titrimetry [12], voltammetry [13] and spectrophotometry [14–15]. From these different approaches, fluorescence is considered the most suitable as a result of its ease of use, cost effectiveness, increased sensitivity and flexible toolbox in the area of environmental monitoring [16–17]. Nevertheless, studies in the field have largely focused on the use of novel fluorophores in monitoring hydrazine including various halo-esters [18–20], keto ester [21–22], acetoxy group [23–27], phthalimide derivative [28–30], active methylene groups [31–34] aldehyde group [35–38] and various other functional groups [39]. Hence, the development of novel fluorophores for the purpose of quantitatively detecting hydrazine in vapor phase is still significantly challenging.

* Corresponding author.
E-mail address: nakorn.nia@kmutt.ac.th (N. Niamnont).

https://doi.org/10.1016/j.jphotochem.2020.112879
Received 13 July 2020; Received in revised form 17 August 2020; Accepted 30 August 2020
Available online 6 September 2020
1010-6030/© 2020 Elsevier B.V. All rights reserved.

Electrospinning is a basic and notable flexible approach that can directly produce nanofibers from various different polymers and composite materials under the application of high voltage [40–41]. The surface to volume ratio of nanofibers is high, thus promoting their successful application in various fields including for sensors [42–43], biomedical and biosensing materials [44–46], electrode materials [47–48], controlled drug delivery [49–50], wound dressings [51–52], oily wastewater separation [53–55] and air filtration [56–57]. Non-woven nanofiber mats exhibit increased porosity and a large surface area, making them perfect for use as scaffolds in sensor applications [58]. Recent studies have reported the use of chemical sensors of fluorophores formed from electrospun nanofibers for a variety of different analytes, including metal ions (Cu^{2+} and Cr^{3+}) [59] explosives [60–61], proteins [62] and volatile organic compounds [63]. The current research focuses on the development of a compound **1** with **CA** via the application of the electrospinning method for selectively detecting hydrazine in vapor phase, and is the first study to attempt such an approach. Compound **1** consisting of an aldehyde group as hydrazine probe was designed and successfully synthesized. The **CA** was chosen as the substrate for its nontoxic, high-performance, and biodegradable material, along with the **CA** which it has been utilized in many previous studies to fabricate the nanofibrous by electrospinning technique [64]. Moreover, examination of the fluorescent images was performed to quantitatively determine the concentration of hydrazine, selectivity test, reversibility test and mechanistic of the probes for hydrazine detection.

2. Experimental

2.1. Materials and solvents

(4-(diphenylamino)phenylboronic acid and 4-brosalicylaldehyde were acquired from Tokyo Chemical Industry (TCI). Cellulose acetate powder, tetrakis(triphenyl phosphine)palladium(0) and Hydrazine monohydrate 64-65% were bought from Sigma-Aldrich. Analytical reagent grade solvents, such as diethyl ether, tetrahydrofuran (THF), dimethylsulfoxide (DMSO), dimethylformamide (DMF), acetone and acetonitrile (MeCN), were bought from RCI Lab scan. Each of the additional reagents were acquired from Sigma-Aldrich, Merck or RCI Lab scan in a non-selective manner and were not additionally purified unless specifically stated. Reactions were all performed in an atmosphere comprised of N_2. Furthermore, monitoring of the reaction's progress was performed with F254 thin layer chromatography (TLC) and visualisation of the components was achieved via observation under UV light (365 nm). Solvents for extraction and chromatography, such as hexane, dichloromethane (DCM), ethyl acetate(EtOAc), were of commercial grade and were distilled before use. All aqueous solutions were prepared using Type II (pure) water.

2.2. Analytical instrument

The ^1H and ^{13}C NMR spectra were conducted for salicylaldehyde derivatives using a Bruker Avance III HD Spectrometer (400 MHz, 100 MHz for ^1H and ^{13}C) where the internal standard used was tetramethylsilane. The amount of absorption signals in the ^1H NMR- spectra was classified in the following manner: s/singlet; d/doublet, t/triplet, sd/singlet of doublet, dd/doublet of doublet, dt/doublet of triplet, td/triplet of doublet, tt/triplet of triplets, m/multiplet. A Thermo Fisher Scientific device (model Nicolet 8700) was used to perform infrared spectra with KBr pellets. High resolution electrospray ionization mass spectra (HRMS) were obtained using a Bruker maXis with ethyl acetate as the solvent in the positive ionisation mode. Measurement of melting points was performed with a Thomas Hoover capillary device and no corrections were subsequently made to the generated values. A Hitachi F-2500 fluorescence spectrophotometer was used to measure the fluorescent spectra. Measurement of UV-Vis absorption spectra was performed with a Perkin Elmer ltd, lambda 35/fias 300 UV-vis spectrophotometer. Finally, a JEOL (JSM-6301 F) SEM analyser was utilised for the analysis of the electrospun nanofibrous sheet's morphology.

2.3. One pot synthesis of compound 1

A combination of (4-(diphenylamino)phenylboronic acid (500.0 mg, 1.72 mmol), tetrakis(triphenyl phosphine)palladium(0) (180 mg, 0.16 mmol), 4-brosalicylaldehyde (346.1 mg, 1.72 mmol) in THF (10 mL) and water (1 mL) was added to K_2CO_3 (500 mg, 3.62 mmol) in an environment of N_2 gas, and stirring of the resulting mixture was performed at 70 ℃. The reaction was allowed to proceed for 4 hours, after which 1 M HCl (20 mL) was added to the mixture and extraction was performed with EtOAC (2 × 15 ml). After being evaporated, the residue was eluted through a column of silica gel via pure hexane to hexane/DCM (2/3) as the eluent to yield a solid with bright yellow colour.

2.4. Photophysical properties of compound 1 in difference solvent polarities

The stock solution compound **1** (1 mM) were dissolved in their solvent ranging from low to high polarities, namely diethyl ether, THF, DMSO, DMF, acetone and MeCN. Subsequently, then diluted concentration of compound **1** from previous will be 20 μM followed by incubation for 10 min under rt conditions. Recording of the UV-Vis absorption was performed in the range between 300 nm and 700 nm, while measurement of the fluorescence spectra was conducted in the range between 390 nm and 700 nm where their maximum absorption wavelength was used as the excitation wavelength.

2.5. Optical spectra respond of compound 1 toward hydrazine

Stock solution compounds **1** (1 mM) were dissolved in DMSO. Dilution was performed for various samples of compounds **1,** where each was prepared individually either included and did not include the hydrazine solution in DSMO. The final concentration of the samples was 20 μM and incubation of the samples was performed at rt for 10 min. The UV-Vis absorption ranged between 300 nm and 700 nm, while measurement of the fluorescence spectra showed values between 390 nm and 700 nm where their maximum absorption wavelength was used as the excitation wavelength.

2.6. Theoretical calculations

Optimisation of the ground-state molecular geometry was achieved by utilizing the density functional theory (**DFT**) through the implementation of the Gaussian 09 program at the B3LYP/6-31G** basis set [65–66]. Determination of optimal geometries was based on isolated entities within a vacuum with no imposition of conformation constraints. Time-dependent density functional theory (**TDDFT**) calculations were performed on the optimised geometries obtained (utilising the identical functional and basis set used in the previous calculations) for the purpose of predicting the vertical electronic excitation energies. Plotting of molecular orbital contours was performed with Gauss View 6.

2.7. Fabrication of compound 1 nanofibrous sheet

The 0.01 %w/v of compound **1** was synthesized via the Suzuki-Miyaura cross-coupling reaction and dissolved in a mixture between 1 %v/v of tween 80 and 2:1 acetone/DMF at ambient temperature. Then, the 17 %w/v of **CA** powder was added into stirred for 1 h until the polymer solution was homogenous. In the electrospinning procedure, the compound **1-CA** polymer solution was fed into a syringe with needle and the standard parameters were as follows [64]: the electric voltage applied was 17 kV, the solution feed rate was 2 mL h-, and the tip of the

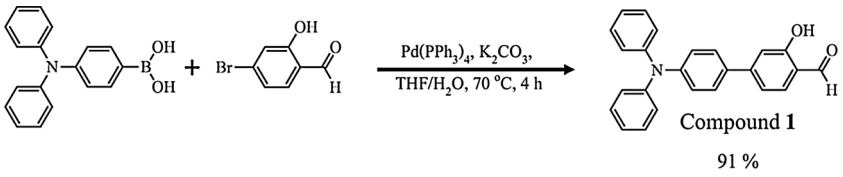

Scheme 1. The one step synthetic route of compound **1**.

needle was positioned at a distance of 12 cm from the collector wheel. After finishing the electrospun nanofibrous sheets, the compound **1** nanofibrous sheets were removed from the collector wheel and performed in a vacuum oven at 60 °C for 6 h for the purpose of remove any remaining solvent. Lastly, gold layers were applied to the nanofibrous sheet via sputter coating and it was subsequently analysed with a JEOL (JSM-6301 F) SEM machine at an accelerating voltage of 20 kV to study the morphology.

*2.8. Hydrazine vapor quantitative detection of compound **1** nanofibrous sheet*

In order to detect hydrazine quantitively in vapour phase, fluorescent images were analysed to evaluate the changes in the fluorescent intensity of the nanofibrous sheets of compound **1** subsequent to being fumigated with hydrazine vapor. Firstly, the nanofibrous sheets of compound **1** were divided into segments with dimensions of 1.5 cm x 1.5 cm. Secondly, photographs of the nanofibrous sheets of compound **1** were captured prior to being exposed to hydrazine vapor using a portable UV lamp with excitation at 365 nm. Thirdly, the sheets were position on the top of a vial that contained hydrazine at different concentrations (0, 0.20, 0.30, 0.40, 0.50, 0.75 and 0.10 %w/v) within an aqueous solution for a period of 10 min; Subsequently, photographs were captured again using a portable UV lamp with an excitation of 365 nm. an iPhone smartphone with the Pro Camera application was used to record the photographic images using the lowest ISO and medium white balance modes. Afterwards, ImageJ (ver. 1.48) software was utilized to covert the digital colour data from the digital photos into greyscale. Lastly, the correlation between the ratio fluorescent image intensity (I/I_0) before (I_0) and after (I) being exposed to hydrazine vapour versus the concentration of hydrazine in the aqueous solution was plotted.

*2.9. Selective and competitive studies of compound **1** nanofibrous sheet*

Photographs of the nanofibrous sheet of compound **1** prior and subsequent to being exposed to various analytes (1%w/v) and adding hydrazine (1%w/v) were captured under a portable UV lamp at an excitation of 365 nm for a fumigation period of 10 min at rt condition. Subsequently, ImageJ (ver. 1.48) software was utilised in order to covert the digital colour data from the digital photos into greyscale. Lastly, the correlation between the ratio fluorescent image intensity (I/I_0) before (I_0) and after (I) being exposed to different analytes was plotted.

*2.10. Sensing mechanism of compound **1** toward hydrazine detection*

^{1}H-NMR titration was utilized to investigate the mechanism of the reaction between compound **1** and hydrazine. Initially, the stock solutions of compounds **1** (20 mM) were dissolved in DMSO-d_6. Dilution of the sample was performed for various samples of compound **1,** each of which contained hydrazine at distinct concentrations (0, 0.5, 1.0, and 2.0 equiv.) in DMSO-d_6, which were prepared individually. The ultimate concentration of the samples was 5 mM and incubation were performed for a period of 10 min under rt conditions. Evaluation of the obtained data was conducted using ^{1}H-NMR spectroscopy and the entire spectra were recombined into a stacked plot using Mnova software.

2.11. Real sample detection

For the practical sample analysis in the laboratory, tap water was preferred. Tap water which has become contaminated from military and industrial wastes, wastewater treatment plant effluents, and possible formation in tap water disinfection processes and distribution systems. Because hydrazine is often used for removal of halogens from wastewater treatment, it may enter drinking water sources that are impacted by wastewater or wastewater treatment plant effluents. Fumigation of the nanofibrous sheet of compound **1** was performed with tap water and the introduction of various concentrations of standard hydrazine solution (0.25, 0.6, 0.9 %w/v). Photographs of the nanofibrous sheet of compound **1** were captured prior and after being exposed to various samples under a portable UV lamp at an excitation of 356 nm with a fumigation period for 10 min at rt conditions. Subsequently, ImageJ (ver 1.48) was utilised to convert digital colour data in the digital photos into greyscale. Lastly, relative standard deviation (RSD%) and recovery percentages were calculated.

3. Results and discussion

3.1. Design and characterization of compound 1

Successful synthesis of the compound **1** was achieved in one step via the Suzuki-Miyaura cross-coupling reaction among (4-(diphenyl amino)

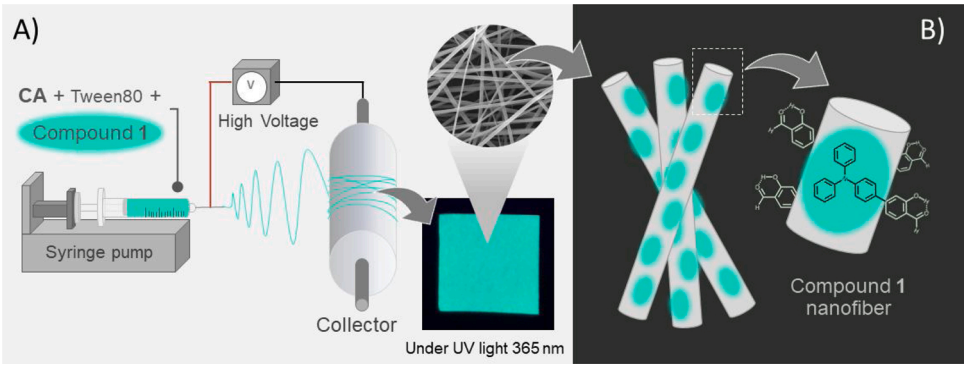

Fig. 1. Fabrication process of the compound **1** (B) mixed with **CA** nanofibrous sheet.

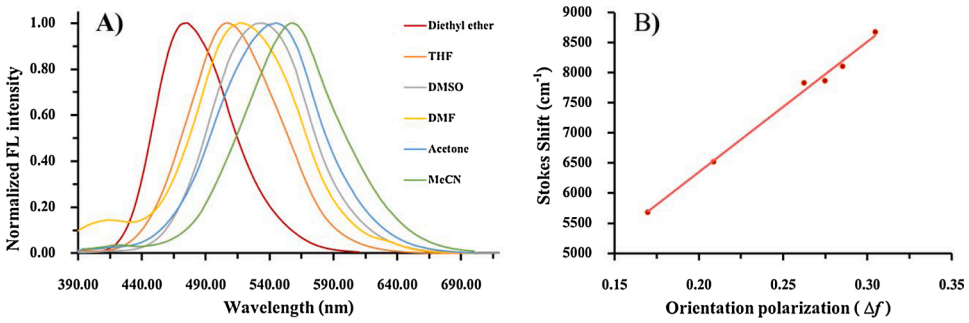

Fig. 2. (A) Normalized fluorescence emission spectra of compound **1** in various solvents at 20 μM using their longest absorption wavelength as excitation wavelength. (B) Lippert-Mataga plots showing the Stokes shift versus the orientation polarization (Δ*f*) of the solvents for compound **1**

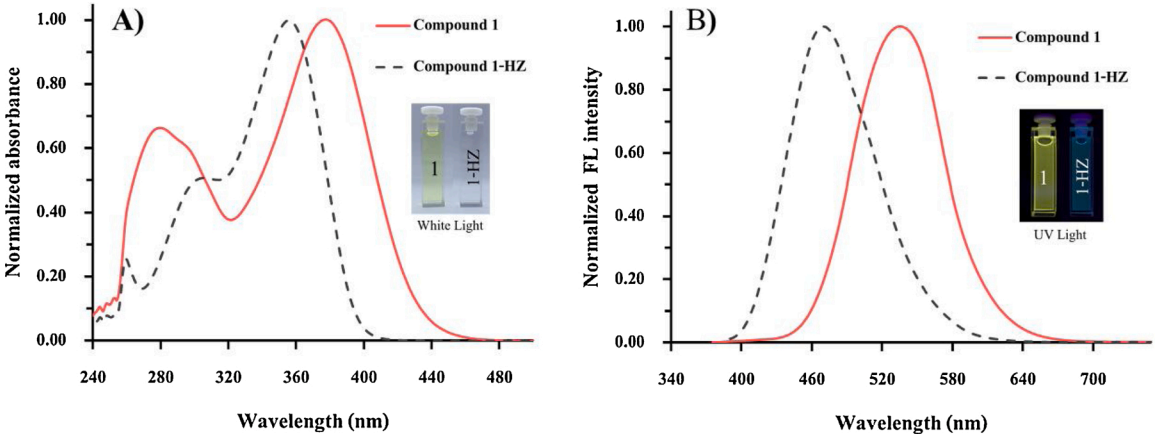

Fig. 3. Changes in normalized absorption (A) and emission spectra (B) for compound **1** (30 μM) before (red line) and after (black line) the addition of N_2H_4 (100 μM) in DMSO. and the inset photo show the colorimetric and fluorogenic changes induced by N_2H_4 treatment, under white light and a 365 nm handheld UV lamp, respectively.

phenyl)boronic acid and 4-Bromo salicylaldehyde to produce an excellent yield of compound **1** (91%), as demonstrated in Scheme 1. The chemical framework of compound **1** includes amine group as an electron donor (**D**) unit with a salicylaldehyde as electron acceptor (**A**) unit that exhibits excellent charge transfer ability, while the formation of a novel fluorescent molecule with a **D**-π–**A** structure occurs. Characterisation and confirmation of compound **1** was performed by ^{1}H-NMR, ^{13}C-NMR, and HRMS information as demonstrated in (Fig S1-S3†). Furthermore, the aldehyde group reacted with nucleophilic targets including hydrazine at rt conditions. Hydrazine attraction causes transformation of formyl into hydrazone, which induces the rupture of the conjugated system and the distribution of electron density. Such a reaction causes distinctive changes in absorption of UV-vis and fluorescence spectra, as well as facilitates fluorogenic and colorimetric detection (Fig. 1).

3.2. *Photophysical properties of compound **1** in difference solvent polarities*

Fig. 2A shows the fluorescence spectra of compound **1** in solvents with distinct polarities. A marginal rise in the emission wavelength was demonstrated in polar solvents to shift compared with those in low polar solvents. This finding implies that the excitation causes the dipole moment of the molecules to increase, while the ground and excited state dipoles exhibit similarities [67–68], suggesting an intramolecular charge transfer (**ICT**) procedure in the molecules throughout optical excitation. Additionally, comparatively good linear correlations exist among the orientation polarization (Δ*f*) of the solvent and Stokes shift (Δυ) where R^2 is calculated as 0.99. It is to confirm the **ICT** process through **D**-π-**A** system from amine as **D** to salicylaldehyde group as **A** of compound **1** by the large stokes shift in high polar solvents [69–70] as shown in Fig. 2B. The emission wavelength shifts as well as the relationship among solvent polarity and emission colour are indications of the potential capacity of compound **1** as a fluorescent probe with the potential to be applied in environmental detection processes.

3.3. *Optical spectral responses of compound **1** toward hydrazine*

To examine the possibility of using compound **1** in the detection of hydrazine, the UV-Vis absorption and fluorescence spectra of compound **1** were analysed both with and without hydrazine, as demonstrated in Fig. 3. Compound **1** exhibits a pair of characteristic absorption bands at 377 nm and 280 nm in DMSO, as illustrated in Fig. 3**A**. These absorption bands can be attributed to the excited-state intramolecular proton-transfer (**ESIPT**) procedure of planar triphenylamine derivatives. A substitute novel individual maximum absorption wavelength emerged at 355 nm, which disrupted the π-conjugation and impact the intramolecular electron density distribution. It was observed that the solution colour transformed from yellow to no color, which allowed hydrazine to be colorimetrically detected via the naked eye.

Hence, when excited at 370 nm, the maximum emission wavelength of compound **1** was 535 nm after hydrazine was added. The intensity of the fluorescence spectra marginally decreased with a blue shift to 455 nm due to the formation of hydrazone by aldehyde and hydrazine, as illustrated in Fig. 3B. Accordingly, the fluorescence color shifted from light yellow to pale blue under UV light at 365 nm (Fig. 3B, inset). The finding indicating the instantaneous formation between compound **1** hydrazine at rt is an advantageous characteristic for the ratio metric fluorescence detection of hydrazine.

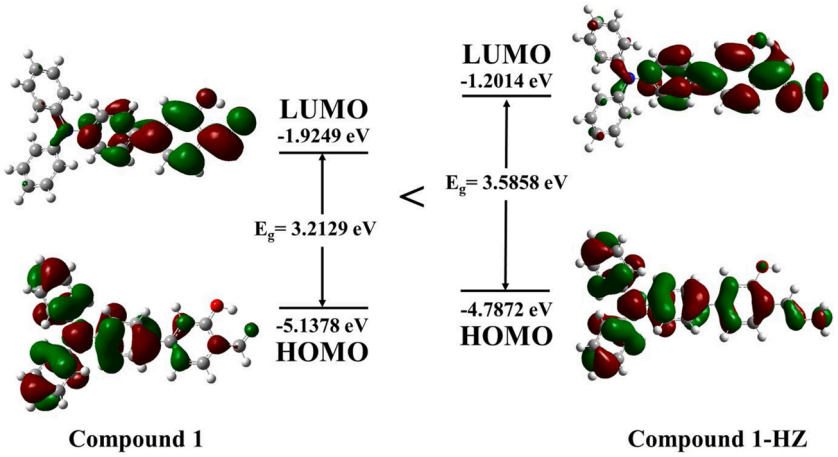

Fig. 4. HOMO-LUMO energy levels and the interfacial plots of the molecular orbitals for compound 1 and its reacted form with hydrazine compound **1-HZ** calculated at the TDDFT level using a B3LYP/6-31G** basis sets in the Gaussian 09 program.

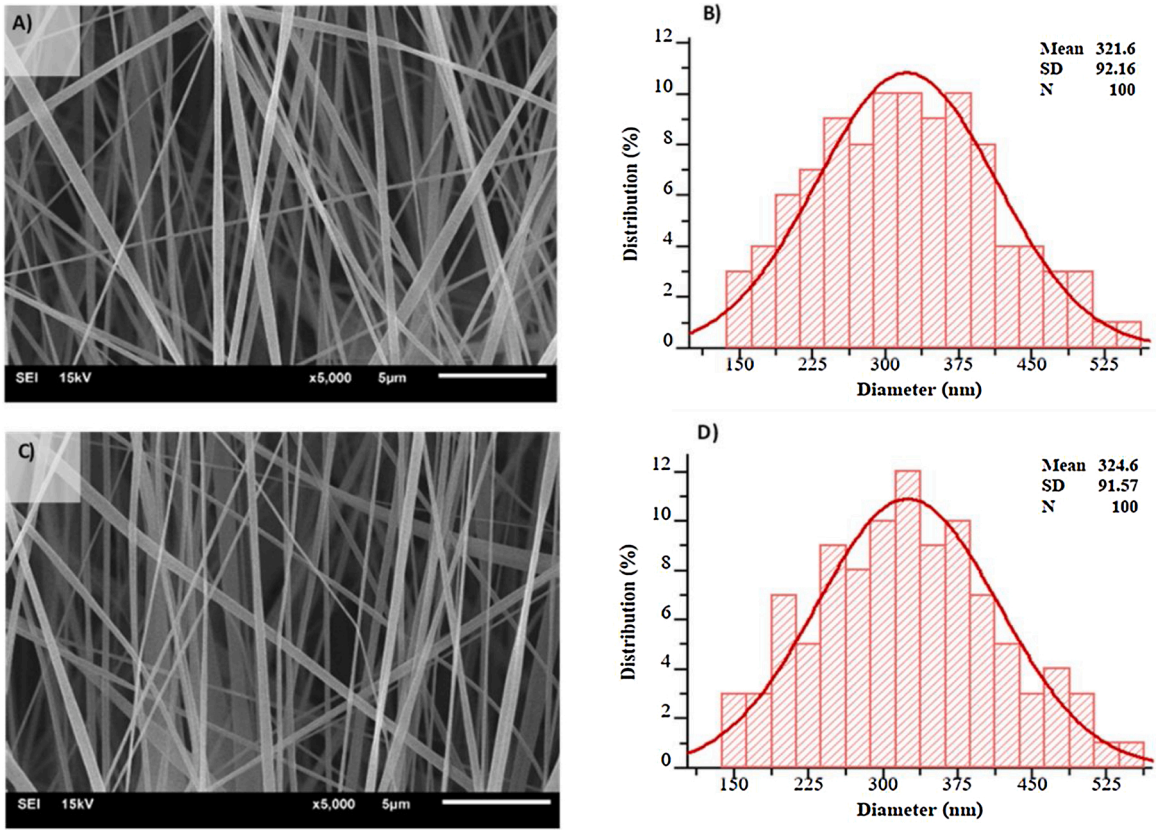

Fig. 5. Typical SEM images and histograms of fiber diameter distribution of pure **CA** of pure **CA** (A and B) nanofibers and compound **1** mixed with **CA** nanofibrous sheet (C and D), respectively.

3.4. Theoretical calculations

To increase the comprehension of the blue shift of the fluorescence response of compound **1** when hydrazine is present, theoretical calculations were performed using **TDDFT** with the B3LYP/6-31G** basis set with the application of a suite of Gaussian 09 software, as illustrated in Fig. 4. The electronic distributions of the compounds prior and after reaction with hydrazine (compound **1** and compound **1-HZ**) are found to significantly different. For compound **1**, the electron densities were localised in the triphenylamine moiety on the highest occupied molecular orbital (**HOMO**) and transitioned to the salicylaldehyde moiety on the lowest unoccupied molecular orbital (**LUMO**). Furthermore, the dispersal of the electron densities across the π-conjugated system on the **HOMO** of the hydrazone product (compound **1-HZ**), but migration to the salicylhydrazone moiety on the **LUMO**. Additionally, calculation of the energy discrepancy between the **HOMO** and **LUMO** of compound **1-HZ** returned a value of 3.5858 eV, while the energy gap for compound **1** was determined to be 3.2129 eV. Hence, the greater energy gap for compound **1-HZ** compared to compound **1** conforms with the blue shift observed in the absorption and emission when compound **1** was treated with hydrazine.

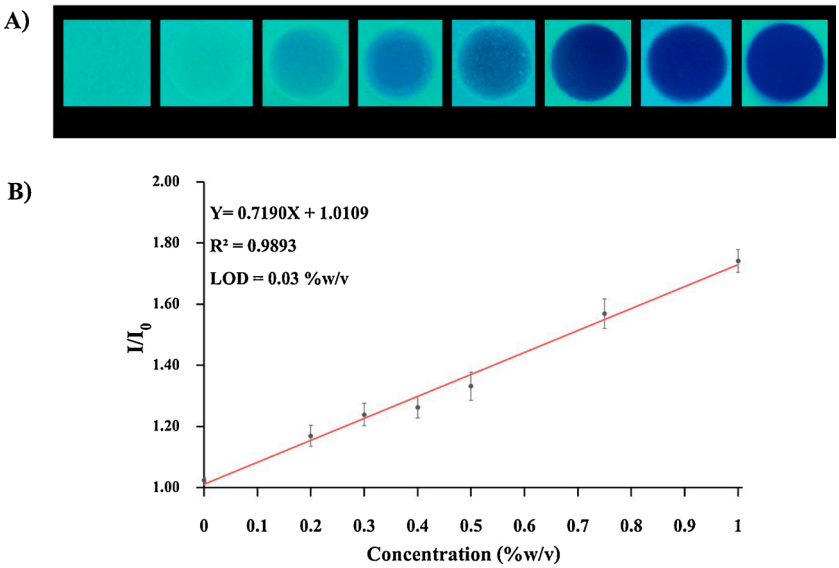

Fig. 6. (A) Fluorescence photo under UV light (365 nm) of compound **1** nanofibrous sheet after fumigation with different concentration of hydrazine aqueous solution. (B) Calibration curves and LOD value of compound **1** nanofibrous sheet (B): Plot of I/I_0 against I and I_0 are the grayscale intensities of fluorescent image before and after fumigation with hydrazine various concentration. Error bars represent mean ± s.d. (n = 5 independent experiments)

3.5. Morphology of compound *1* nanofibrous sheet

The standard SEM images of the electrospun nanofibrous sheet formed from the pure **CA** (A) and compound **1** (0.01%w/v) combined with **CA** (C) are displayed in Fig. 5. Adding compound **1** to the nanofibers does not impact the morphology while nanofibers generated a non-woven mat with a random orientation created space between the nanofibers. Hence, the nanofibers formed from mixing compound **1** with **CA** are uniform and bead free on surface of nanofiber sheet. The data provided in Fig. 5B indicates that the nanofibers had an average diameter of 324.6 ± 91.6 nm. Moreover, mechanical properties of compound **1** nanofibrous sheet were studied as shown in Figure S8. Evidently, this 3-dimensional (3-D) nanoarchitecture utilises a basic electrospinning approach. It is anticipated that the increased surface areas surrounding and inside the porous nanofiber film can potentially offer atypically elevated sensitive and rapid response times for sensing applications [71].

3.6. Hydrazine vapor quantitative detection of compound *1* nanofibrous sheet

For the purpose of developing methods for easily and efficiently detecting hydrazine, preparation of the nanofibrous sheet of compound **1** was performed with the electrospinning method and it was

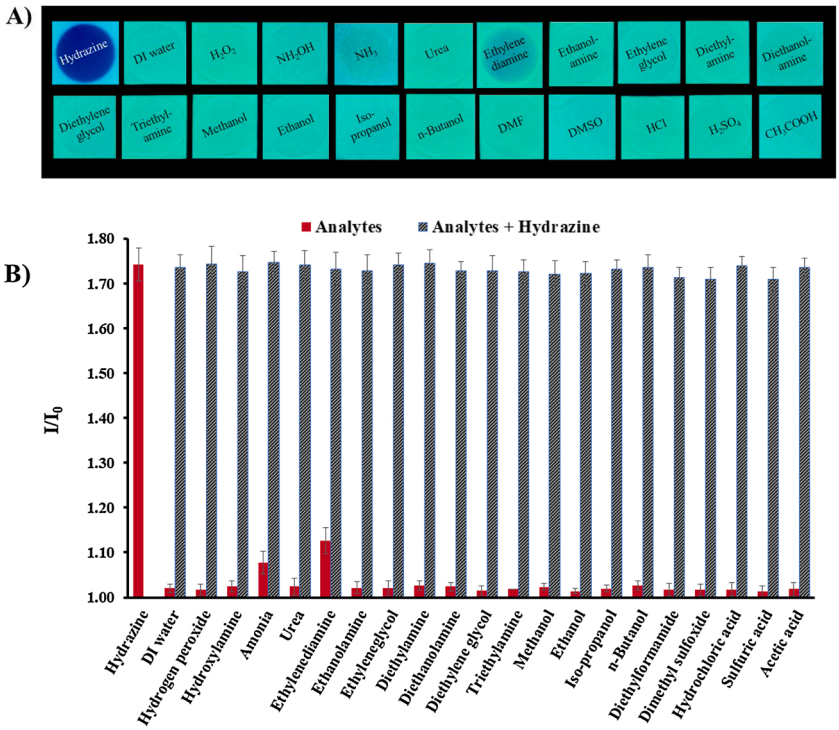

Fig. 7. (A) Fluorescence photo under UV light (365 nm) of compound **1** nanofibrous sheet after 10 min of fumigation with various analytes at r.t. (B) Florescence image intensity ratio (I/I_0) of compound **1** nanofibrous sheet expose for 10 min at r.t. with several analytes (1%w/v) and the addition of hydrazine (1%w/v): Hydrazine (1), DI water (2), hydrogen peroxide (3), hydroxylamine (4), sodium hydroxide (5), sodium bicarbonate (6), ammonia (7), urea(8), ethylenediamine(9), ethanolamine (10), ethylene glycol (11), diethanolamine (12), diethanolamine (13), diethylene glycol (14), triethylamine (15), methanol (16), ethanol (17), iso-propanol (18), n-butanol (19), dimethylformamide (20), dimethyl sulfoxide (21), hydrochloric acid(22), sulfuric acid (23) and acetic acid (24).

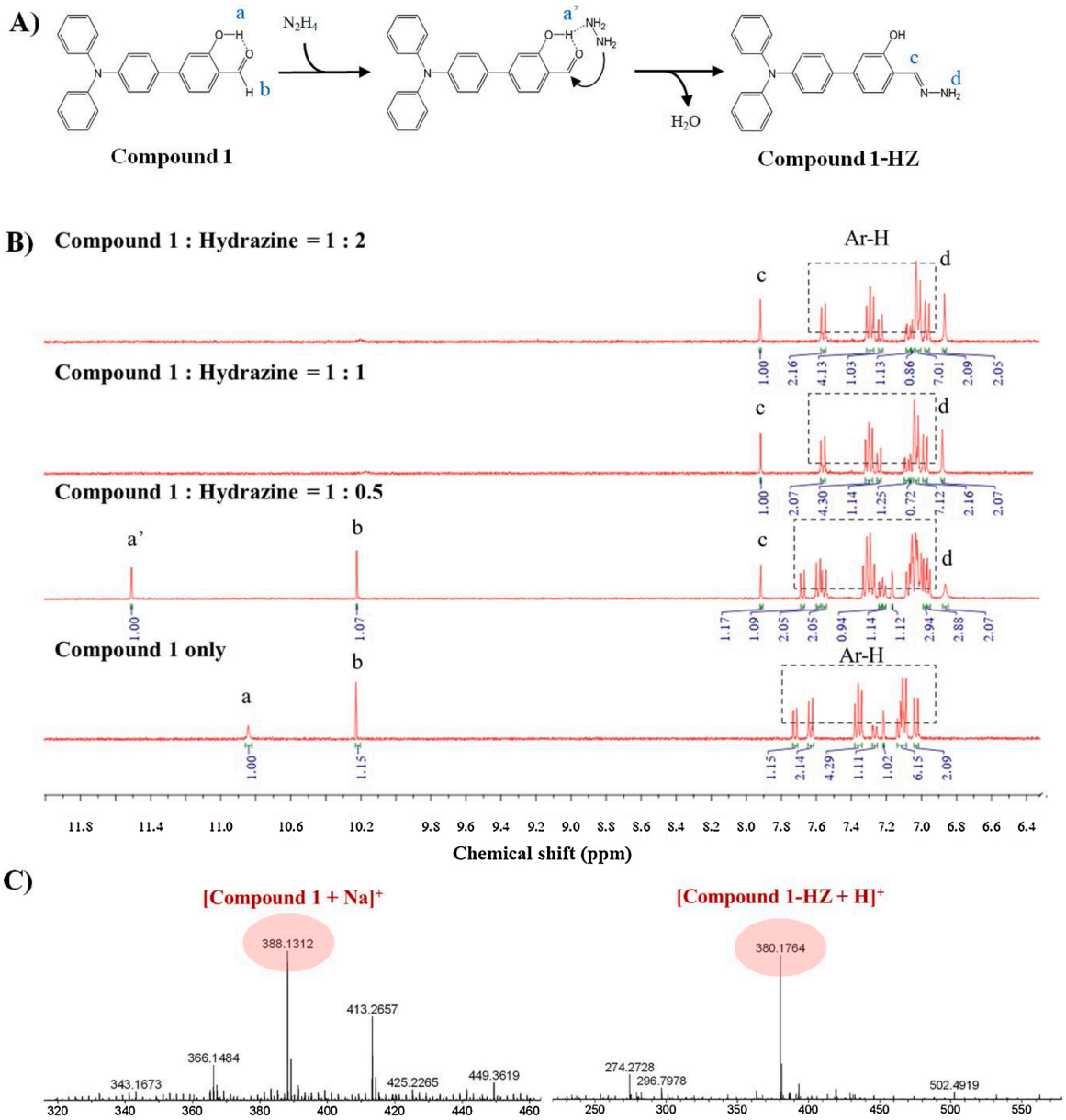

Fig. 8. Sensing mechanism of compound **1** to hydrazine detection. (A) Reaction scheme representing the formation of the hydrazone (compound **1-HZ**). (B) ^{1}H NMR spectra titration of compound **1** (10 μM) upon addition of various equivalents (0, 0.5, 1 and 2 equiv.) in DMSO-d_6. (C) ESI-HRMS of compound **1** and (D) ESI-HRMS of compound **1-HZ**.

subsequently divided into segments with dimensions of 1.5 cm x 1.5 cm. The nanofibrous sheet of compound **1** was placed at the opening of a vial that contained an aqueous solution of hydrazine and was then fumigated for 10 min at rt as illustrated in Fig. 6A. The fluorescent emissions of the nanofibrous sheet diminished from a powerful green light to a signal with no fluorescence based on the hydrazine concentration within the aqueous solution. In order to discriminate hydrazine, a smart phone was used to capture photographs of the fluorescent images under a portable UV lamp at an excitation of 365 nm. Subsequently, the ImageJ (ver 1.48) programme was utilised to convert digital colour information from the digital photographs into grayscale values. Lastly preparation of the calibration curve was made by plotting the ratio fluorescent image density (I/I_0) prior (I_0) and subsequent (I) to being exposed to hydrazine vapor for different concentrations of hydrazine (0.2, 0.3, 0.4, 0.5, 0.75 and 1.0%w/v) in an aqueous solution as shown in Fig. 6B. The concentration ranged linearly from 0.2-1.0 %w/v. The limit of detection (**LOD**) for hydrazine was determined to be 0.03 %w/v (~ 9 mM) utilising the conventional technique (3 s/K, s = standard derivation of blank, K = slope of calibration), which seemed to be the optimal value lower than has been reported by previous experiments (see Table S1).

*3.7. Vapor phase selectivity and competition of compound **1** nanofibrous sheet*

The selectivity study of the nanofibrous sheet of compound **1** towards hydrazine vapor was additionally investigated by utilizing 22 compounds, including Hydrazine (1), DI water (2), hydrogen peroxide (3), hydroxylamine (4), ammonia (5), urea(6), ethylenediamine(7), ethanolamine(8), ethylene glycol (9), diethanolamine (10), diethanolamine (11), diethylene glycol (12), triethylamine (13), methanol (14), ethanol (15), iso-propanol (16), n-butanol (17), dimethylformamide (18), dimethyl sulfoxide (19), hydrochloric acid(20), sulfuric acid (21) and acetic acid (22). The findings indicate that the emissions of compound **1** did not change significantly in fluorescent mode with various

Table 1
The percent recovery data for the detection of hydrazine in spiked tap water samples ((n = 3)[a]. ([a]Mean ± SD).

Sample	Found (%w/v)	Spike (%w/v)	Found (%w/v)	Recovery (%)	RSD (%)
Tap water	0.01 ± 0.01	0.25	0.26 ± 0.01	102.2	4.5
		0.60	0.62 ± 0.03	103.4	4.8
		0.90	0.89 ± 0.04	98.8	4.0

amines, volatile organic compounds, acids and bases analytes under the same conditions. It is interesting to note that the emissions of compound **1** only showed a significant decrease when hydrazine vapour was present, as demonstrated in Fig. 7. It was also possible to observe the particular reaction of the nanofibrous sheet of compound **1** to hydrazine vapour via the naked eye (Fig. 7). Furthermore, interference studies were conducted on additional competitive anions to verify that the probe is capable of purely detecting hydrazine when a large number of other molecules are present.

3.8. Sensing mechanism of compound *1* to hydrazine detection

The sensing mechanism of the interaction between hydrazine and compound **1** was examined via contracting various experimental analyses (Fig. 8**A**). Fig. 8**B** shows the ^{1}H NMR titration spectra of compound **1** (10 μM) after adding several equivalents (0, 0.5, 1 and 2 equiv.) in DMSO-d_6. When hydrazine was not present, Compound **1** exhibited an aldehyde proton at 10.23 ppm (b-H) as well as an hydroxyl proton at 10.84 ppm (a-H), which was caused by the **ESIPT** when an intramolecular hydrogen bond (H-bond) was present between the proton donor (–OH) and the proton acceptor (–C = O) groups. Subsequent to the addition of excess hydrazine, the aldehyde proton (b-H) was no longer detected, indicating that aldehyde was substituted with hydrazine. Hydrazine formed a Schiff base and **ESIPT** was obstructed. Furthermore, emergence of the new chemical shifts for the = CH- and -NH_2 group occurred at 7.95 (c-H) and 6.92 ppm (d-H), respectively. ESI-MS analysis was conducted on the hydrazine Schiff base (compound **1-HZ**), and the results showed that (compound **1-HZ**) was subjected to (m/z = 380.1764 for $C_{25}H_{21}N_3O$, [compound **1-HZ**+H]$^+$), which correspond to the calculation(m/z = 380.1763) (Fig. 8**C**).

3.9. Real water sample

The nanofibrous sheet of compound **1** was employed to monitor hydrazine in samples of tap water. Each of the samples was spiked with a determined volume of hydrazine (0.1 %w/v). Every sample was tested three times and the findings are demonstrated in Table 1. This technique had increased analytical precision (RSD < 5%) and acceptable accuracy (< 5% error), thus suggesting that it has reliability for the detection of hydrazine in actual samples. Compared with different fluorophores utilised for detecting hydrazine in water media, compound **1** has a lower detection threshold (Table **S1**). The reusability and reproducibility of the nanofibrous mat was also investigated. To determine, the reusability of the nanofibrous mat sensor, the compound **1** nanofibrous sheet was controlled by alternating the fumigation of 1%v/v N_2H_4 and the immersion of 5%wt HCl. The nanofibrous mat was then reused for sensing the hydrazine vapor as shown in Figure **S9**. The result showed that the compound **1** nanofibrous sheet was reused over 4 times. Hence, this finding indicates the nanofibrous sheet of compound **1** has potential for use as new option for selectively detecting hydrazine vapor.

4. Conclusion

In summary, this study presents the successful development of a novel triphenylamine based salicylaldehyde fluorophore (compound **1**) combined with a **CA** electrospun nanofibrous sheet for quantitatively detecting hydrazine in vapor phase. The nanofibrous sheet exhibits multiple functionalities as it acts as a fluorescence quencher and chemo selective toward hydrazine. For the purposes of convenience, we applied fluorescence image analysis to the nanofibrous sheet using Image J software, which enabled the concentration of hydrazine to be effectively determined by just examining the changes in the intensity of the fluorescent images. In comparison to different solid state fluorogenic for the detection of hydrazine gases, the proposed nanofibrous sheet could offer an easy but advantageous technique for practically detecting chemicals in environmental settings. The detection threshold for hydrazine vapor for the nanofibrous sheet of compound **1** was 0.03 %w/v. Accordingly, Compound **1** showed selectivity and sensitive to hydrazine, while the turn-off mode of detection materialised via a reduced **ESPIT** procedure induced by hydrazine. Additionally, the reusability of nanofiber sheet exhibited less than 15% change of signal change in a 4-cycle test for hydrazine vapor detection. Lastly, it is possible to achieve acceptable results by applying Compound **1** for the detection of hydrazine in actual samples of water.

CRediT authorship contribution statement

Apisit Karawek: Conceptualization, Formal analysis, Visualization, Writing - original draft. **Pipattra Mayurachayakul:** Investigation, Writing - review & editing. **Thanapich Santiwat:** Investigation, Writing - review & editing. **Mongkol Sukwattanasinitt:** Conceptualization, Writing - review & editing. **Nakorn Niamnont:** Conceptualization, Supervision, Conceptualization, Formal analysis, Writing - review & editing.

Declaration of Competing Interest

The authors reported no declarations of interest.

Acknowledgments

This work was supported by Thailand Research Fund under grants MRG6180070 and RTA6180007. A.K. is grateful to the research fund for Petchra Pra Jom Klao Master Scholarship for Master's student of King Mongkut's University of Technology Thonburi (KMUTT).

Appendix A. Supplementary data

Supplementary material related to this article can be found, in the online version, at doi:https://doi.org/10.1016/j.jphotochem.2020.112879.

References

[1] A. Furst, R.C. Berlo, S. Hooton, Hydrazine as a reducing agent for organic compounds (catalytic hydrazine reductions), Chem. Rev. 65 (1965) 51–68.
[2] J.R. Dilworth, The coordination chemistry of substituted hydrazines, Coord. Chem. Rev. 21 (1976) 29–62.
[3] J. Wang, L. Chen, Hydrazine detection using a tyrosinase-based inhibition biosensor, Anal. Chem. 67 (1995) 3824–3827.
[4] S.C. Moldoveanu, Pyrolysis of Organic Molecules, Second Edition, Elsevier, 2019, pp. 349–390.
[5] M. Blackand, H. Hussain, Hydrazine, cancer, the Internet, isoniazid, and the liver, Int. Med. 133 (2000) 911–913.
[6] Y. Tan, J. Yu, J. Gao, Y. Cui, Y. Yang, G. Qian, A new fluorescent and colorimetric probe for trace hydrazine with a wide detection range in aqueous solution, Dyes Pigm. 99 (2013) 966–971.
[7] Vernot E.H, J.D. MacEwen, R.H. Bruner, C.C. Haun, E.R. Kinkead, D.E. Prentice, A. Hall, R.E. Schmidt, R.L. Eason, G.B. Hubbard, J.T. Young, Long-term inhalation toxicity of hydrazine, Fund Appl. Toxicol. 5 (1985) 1050–1064.
[8] S. Garrod, M.E. Bollard, A.W. Nicholls, S.C. Connor, J. Connelly, J.K. Nicholson, E. Holmes, Integrated Metabonomic Analysis of the Multiorgan Effects of Hydrazine Toxicity in the Rat, Chem. Res. Toxicol. 18 (2005) 114–122.
[9] S.D. Zelnick, D.R. Mattie, P.C. Stepaniak, Occupational exposure to hydrazines: treatment of acute central nervous system toxicity, Aviat. Space Environ. Med. 74 (2003) 1285–1291.

[10] X. Chen, X. Xiang, Z. Li, A. Tong, Sensitive and selective fluorescence determination of trace hydrazine in aqueous solution utilizing 5-chlorosalicylaldehyde, Anal. Chim. Acta 625 (2008) 41–46.
[11] M. Georgea, K.S. Nagaraja, N. Balasubramanian, Spectrophotometric determination of hydrazine, Talanta 75 (2008) 27–31.
[12] J.D. Clark, J.R. Smith, Titrimetric Analysis of Mixtures of Hydrazine and Methyl Hydrazine, Anal. Chem. 33 (1961) 1186–1187.
[13] C.H. Chen, L. Jacobse, K. McKelvey, C.S.L. Lai, M.T.M. Koper, P.R. Unwin, Voltammetric scanning electrochemical cell microscopy: dynamic imaging of hydrazine electro-oxidation on platinum electrodes, Anal. Chem. 87 (2015) 5782–5789.
[14] K. Ravichandran, R.P. Baldwin, Liquid chromatographic determination of hydrazines with electrochemically pretreated glassy carbon electrodes, Anal. Chem. 55 (1983) 1782–1786.
[15] A.D. Smolenkov, O.A. Shpigun, Direct liquid chromatographic determination of hydrazines: A review, Talanta 102 (2012) 93–100.
[16] Y. Jung, N.K. Park, J.S. Kang, D. Kim, Hydrazine-Selective Fluorescent Turn-On Probe Based on Ortho-Methoxy-Methyl-Ether (o-MOM) Assisted Retro-aza-Henry Type Reaction, Sensors 19 (2019) 4525.
[17] Y. Xie, L. Yan, Y. Tang, M. Tang, S. Wang, L. Bi, W. Sun, J. Li, A Smart Fluorescent Probe Based on Salicylaldehyde Schiff`s Base with AIE and ESIPT Characteristics for the Detections of N_2H_4 and ClO, J. Fluoresc. 29 (2019) 399–406.
[18] X. Jin, C. Liu, X. Wang, H. Huang, X. Zhang, A flavone-Based ESIPT fluorescent sensor for Detection of N_2H_4 in aqueous solution and gas state and its imaging in living cells, Sens. Actuators B Chem. 216 (2015) 141–149.
[19] Y. Hao, Y. Zhang, K. Ruan, W. Chen, B. Zhou, X. Tan, Y. Wang, L. Zhao, G. Zhang, P. Qu, M. Xu, A naphthalimide-based chemodosimetric probe for ratiometric detection of hydrazine, Sens. Actuators B Chem. 244 (2017) 417–424.
[20] X. Jiang, M. Shangguan, Z. Lu, S. Yi, X. Zeng, Y. Zhang, L. Hou, A "turn-on" fluorescent probe based on V-shaped bis-coumarin for detection of hydrazine, Tetrahedron 76 (2020) 130921.
[21] M.G. Choi, J. Hwang, L.O. Moon, J. Sung, S.K. Chang, Hydrazine-selective chromogenic and fluorogenic probe based on levulinated coumarin, Org. Lett. 13 (2011) 5260–5263.
[22] S. Yu, S. Wang, H. Yu, Y. Feng, S. Zhang, M. Zhu, H. Yin, X. Meng, A ratiometric two-photon fluorescent probe for hydrazine and its applications, Sens. Actuators B Chem. 220 (2015) 1338–1345.
[23] Y. Sun, D. Zhao, S. Fan, L. Duan, A new near-infrared ratiometric fluorescent probe for hydrazine, Sens. Actuators B Chem. 208 (2015) 512–517.
[24] X. Xia, F. Zeng, P. Zhang, J. Lyu, Y. Huang, S. Wu, An ICT-based ratiometric fluorescent probe for hydrazine detection and its application in living cells and in vivo, Sens. Actuators B Chem. 227 (2016) 411–418.
[25] A.K. Mahapatraa, P. Karmakara, S. Mannaa, K. Maitia, D. Mandal, Benzthiazole-derived chromogenic, fluorogenic and ratiometric probes for detection of hydrazine in environmental samples and living cells, J. Photochem. Photobiol. A 334 (2017) 1–12.
[26] X. Kong, B. Dong, C. Wang, N. Zhang, W. Song, W. Lin, A novel mitochondria-targeted fluorescent probe for imaging hydrazine in living cells, tissues and animals, J. Photochem. Photobiol. A 356 (2018) 321–328.
[27] J. Wu, J. Pan, Z. Ye, L. Zeng, D. Su, A smart fluorescent probe for discriminative detection of hydrazine and bisulfite from different emission channels, Sens. Actuators B Chem. 274 (2018) 274–284.
[28] L. Cui, Z. Peng, C. Ji, J. Huang, D. Huang, J. Ma, S. Zhang, X. Qian, Y. Xu, Hydrazine detection in the gas state and aqueous solution based on the Gabriel mechanism and its imaging in living cells, Chem. Commun. 50 (2018) 1485–1487.
[29] L. Cui, C. Ji, Z. Peng, L. Zhong, C. Zhou, L. Yan, S. Qu, S. Zhang, C. Huang, Z. Qian, Y. Xu, Unique Tri-Output Optical Probe for Specific and Ultrasensitive Detection of Hydrazine, Anal. Chem. 86 (2014) 4611–4617.
[30] F. Ali, H.A. Anila, N. Taye, D.G. Mogare, S. Chattopadhyay, A. Das, Specific Receptor for Hydrazine: Mapping the in Situ Release of Hydrazine in Live Cells and in an in Vitro Enzymatic Assay, Chem. Commun. 52 (2016) 6166–6169.
[31] M. Sun, J. Guo, Q. Yang, N. Xiao, Y. Lia, A new fluorescent and colorimetric sensor for hydrazine and its application in biological systems, J. Mater. Chem. B 2 (2014) 1846–1851.
[32] S.K. Samanta, K. Maiti, S.S. Ali, U.N. Guria, A. Ghosh, P. Datta, A.K. Mahapatra, A solvent directed D-π-A fluorescent chemodosimeter for selective detection of hazardous hydrazine in real water sample and living cell, Dyes Pigm. 173 (2020) 107997.
[33] R.C. Gupta, S.K. Dwivedi, R. Ali, S.S. Razi, R. Tiwari, S. Krishnamoorthi, M. Misra, A sensitive TICT Probe exhibiting ratiometric fluorescence repose to detect hydrazine in solution and gas phase, Spectrochim. Acta A 232 (2020) 118153.
[34] R. Zhang, C.J. Zhang, Z. Song, J. Liang, R.T.K. Kwok, B.Z. Tang, B. Liu, AIEgens for real-time naked-eye sensing of hydrazine in solution and on a paper substrate: structure-dependent signal output and selectivity, J. Mater. Chem. C 4 (2016) 2834–2842.
[35] L. Xiao, J. Tu, S. Sun, Z. Pei, Y. Pei, Y. Pang, Y. Xu, A fluorescent probe for hydrazine and its in vivo applications, RCS Adv. 79 (2014) 41807–41811.
[36] J. Cui, G. Gao, H. Zhao, Ya. Liu, H. Nie, X. Zhang, A highly sensitive and selective fluorescent probe for N2H4 in air and living cells, New J. Chem. 41 (2017) 11891–11897.
[37] W. Xu, W. Liu, T. Zhou, Y. Yang, W. Li, A novel PBT-based fluorescent probe for hydrazine detection and its application in living cells, J. Photochem. Photobiol. A 356 (2018) 610–616.
[38] N. Meher, P. Swagatika, S. Kumar, P.K. Iyer, Aldehyde group driven aggregation-induced enhanced emission in naphthalimides and its application for ultradetection of hydrazine on multiple platforms, Chem. Sci. 9 (2018) 3978–3985.
[39] H. Wang, Y. Li, S. Yang, H. Tian, Y. Liu, B. Sun, A dual-function fluorescent probe for discriminative detection of hydrogen sulfide and hydrazine, J. Photochem. Photobiol. A 377 (2019) 36–42.
[40] N. Bhardwaj, S.C. Kundu, Electrospinning: A fascinating fiber fabrication technique, Biotechnol. Adv. 28 (2010) 325–347.
[41] J. Xue, T. Wu, Y. Dai, Y. Xia, Electrospinning and Electrospun Nanofibers: Methods, Materials, and Applications, Chem. Rev. 119 (2019) 5298–5415.
[42] D.S. Sutara, N. Padmaa, D.K. Aswala, S.K. Deshpandeb, S.K. Guptaa, J.V. Yakhmia, Preparation of nanofibrous polyaniline films and their application as ammonia gas sensor, Sens. Actuators B Chem. 128 (2017) 286–292.
[43] S. Jo, J. Kim, J. Noh, D. Kim, G. Jang, N. Lee, E. Lee, T.S. Lee, Conjugated Polymer Dots-on-Electrospun Fibers as a Fluorescent Nanofibrous Sensor for Nerve Gas Stimulant, ACS Appl. Mater. Interfaces 6 (2014) 22884–22893.
[44] B.W. Davis, N. Niamnont, C.D. Hare, M. Sukwattanasinitt, Q. Cheng, Nanofibers Doped with Dendritic Fluorophores for Protein Detection, ACS Appl. Mater. Interfaces 2 (2010) 1798–1803.
[45] Y. Loo, S. Zhang, C.A. Hauser, From short peptides to nanofibers to macromolecular assemblies in biomedicine, Biotechnol. Adv. 30 (2012) 593–603.
[46] S. Qianab, L. Songb, L. Sunb, X. Zhangb, Z. Xina, J. Yinbc, S. Luanbc, Metal-organic framework/poly (ε-caprolactone) hybrid electrospun nanofibrous membranes with effective photodynamic antibacterial activities, J. Photochem. Photobiol. A 400 (2020) 112626.
[47] H. Wang, W. Wang, H. Wang, X. Jin, H. Niu, H. Wang, H. Zhou, T. Lin, High Performance Supercapacitor Electrode Materials from Electrospun Carbon Nanofibers in-situ Activated by High Decomposition Temperature Polymer, ACS Appl. Energy Mater. 1 (2018) 431–439.
[48] J. Han, S. Wang, S. Zhu, C. Huang, Y. Yue, C. Mei, X. Xu, C. Xia, Electrospun Core−Shell Nanofibrous Membranes with Nanocellulose-Stabilized Carbon Nanotubes for Use as HighPerformance Flexible Supercapacitor Electrodes with Enhanced Water Resistance, Thermal Stability, and Mechanical Toughness, ACS Appl. Mater. Interfaces 11 (2019) 44624–44635.
[49] Z. Liu, F. Wang, B. Gao, F. Chen, Q. Zhang, R. Xiong, J. Han, S.K. Samal, S.C. D. Smedt, C. Huang, pH responsive polyurethane (core) and cellulose acetate phthalate (shell) electrospun fibers for intravaginal drug delivery, Carbohydr. Polym. 151 (2016) 1240–1244.
[50] A. Celebioglu, T. Uyar, Fast Dissolving Oral Drug Delivery System Based on Electrospun Nanofibrous Webs of Cyclodextrin/Ibuprofen Inclusion Complex Nanofibers, Mol. Pharm. 16 (2019) 4387–4398.
[51] Q. Chen, J. Wu, Y. Liu, Y. Li, C. Zhang, W. Qi, K.W.K. Yeung, T.M. Wong, X. Zhao, H. Pan, Electrospun chitosan/PVA/bioglass Nanofibrous membrane with spatially designed structure for accelerating chronic wound healing, Mater. Sci. Eng. C 105 (2019) 110083.
[52] J. He, Y. Liang, M. Shi, B. Guo, Anti-oxidant electroactive and antibacterial nanofibrous wound dressings based on poly(ε-caprolactone)/quaternized chitosan-graft-polyaniline for full-thickness skin wound healing, Chem. Eng. J. 385 (2020) 123464.
[53] Z. Liu, W. Ma, M. Zhang, Q. Zhang, R. Xiong, C. Huang, Fabrication of superhydrophobic electrospun polyimide nanofibers modified with polydopamine and polytetrafluoroethylene nanoparticles for oil–water separation, J. Appl. Polym. Sci. 136 (2019) 47638.
[54] M. Zhang, W. Ma, S. Wu, G. Tang, J. Cui, Q. Zhang, F. Chen, R. Xiong, C. Huang, Electrospun frogspawn structured membrane for gravity-driven oil-water separation, J. Colloid Interface Sci. 547 (2019) 136–144.
[55] M. Zhang, W. Ma, J. Cui, S. Wu, J. Han, Y. Zou, C. Huang, Hydrothermal synthesized UV-resistance and transparent coating composited superoloephilic electrospun membrane for high efficiency oily wastewater treatment, J. Hazard. Mater. 383 (2020) 121152.
[56] D. Weiss, D. Skrybeck, H. Misslitz, D. Nardini, A. Kern, K. Kreger, H.-W. Schmidt, Tailoring Supramolecular Nanofibers for Air Filtration Applications, ACS Appl. Mater. Interfaces 18 (2016) 14885–14892.
[57] D. Lv, R. Wang, G. Tang, Z. Mou, J. Lei, J. Han, S.D. Smedt, R. Xiong, C. Huang, Ecofriendly Electrospun Membranes Loaded with Visible-LightResponding Nanoparticles for Multifunctional Usages: Highly Efficient Air Filtration, Dye Scavenging, and Bactericidal Activity, ACS Appl. Mater. Interfaces 11 (2019) 12880–12889.
[58] X. Wang, Y. Li, B. Ding, "Electrospun Nanofiber-Based Sensors" Electrospun Nanofibers for Energy and Environmental Applications. Nanostructure Science and Technology, Springer, Berlin, Heidelberg, 2014, pp. 267–297.
[59] M. Wang, G. Meng, Q. Huang, Y. Qian, Electrospun 1,4-DHAQ-Doped Cellulose Nanofiber Films for Reusable Fluorescence Detection of Trace Cu^{2+} and Further for Cr^{3+}, Environ. Sci. 46 (2012) 367–373.
[60] Y. Long, H. Chen, Y. Yang, H. Wang, Y. Yang, N. Li, K. Li, J. Pei, F. Liu, Electrospun Nanofibrous Film Doped with a Conjugated Polymer for DNT Fluorescence Sensor, Macromolecules 42 (2009) 6501–6509.
[61] Y. Yang, H. Wang, K. Su, Y. Long, Z. Peng, N. Lia, F. Liu, A facile and sensitive fluorescent sensor using electrospun nanofibrous film for nitroaromatic explosive detection, J. Mater. Chem. 21 (2011) 11895–11900.
[62] B.W. Davis, N. Niamnont, R. Dillon, C.J. Bardeen, M. Sukwattanasinitt, Q. Cheng, FRET Detection of Proteins Using Fluorescently Doped Electrospun Nanofibers and Pattern Recognition, Langmuir 27 (2011) 6401–6408.
[63] B.W. Davis, A.J. Burris, N. Niamnont, C.D. Hare, C.Y. Chen, M. Sukwattanasinitt, Q. Cheng, Dual-Mode Optical Sensing of Organic Vapors and Proteins with Polydiacetylene (PDA)-Embedded Electrospun Nanofibers, Langmuir 30 (2014) 9616–9622.
[64] J. Nootem, P. Chalorak, K. Meemon, W. Mingvanish, K. Pratumyot, L. Ruckthong, C. Srisuwannaket, N. Niamnont, Electrospun cellulose acetate doped with

astaxanthin derivatives from Haematococcus pluvialis for in vivo anti-aging activity, RCS Adv. 8 (2018) 37151–37158.

[65] M.J. Frisch, G.W. Trucks, H.B. Schlegel, G.E. Scuseria, M.A. Robb, J.R. Cheeseman, G. Scalmani, V. Barone, B. Mennucci, G.A. Petersson, H. Nakatsuji, M. Caricato, X. Li, H.P. Hratchian, A.F. Izmaylov, J. Bloino, G. Zheng, J.L. Sonnenberg, M. Hada, M. Ehara, K. Toyota, R. Fukuda, J. Hasegawa, M. Ishida, T. Nakajima, Y. Honda, O. Kitao, H. Nakai, T. Vreven, J.A. Montgomery Jr., J.E. Peralta, F. Ogliaro, M. Bearpark, J.J. Heyd, E. Brothers, K.N. Kudin, V.N. Staroverov, R. Kobayashi, J. Normand, K. Raghavachari, A. Rendell, J.C. Burant, S.S. Iyengar, J. Tomasi, M. Cossi, N. Rega, J.M. Millam, M. Klene, J.E. Knox, J.B. Cross, V. Bakken, C. Adamo, J. Jaramillo, R. Gomperts, R.E. Stratmann, O. Yazyev, A.J. Austin, R. Cammi, C. Pomelli, J.W. Ochterski, R.L. Martin, K. Morokuma, V.G. Zakrzewski, G.A. Voth, P. Salvador, J.J. Dannenberg, S. Dapprich, A.D. Daniels, Ö. Farkas, J. B. Foresman, J.V. Ortiz, J. Cioslowski, D.J. Fox, Gaussian 09, Revision **E.01**, Gaussian, Inc., Wallingford CT, 2009.

[66] H.B. Hassan, Density Function Theory B3LYP/6-31G** Calculation of Geometry Optimization and Energies of Donor-Bridge-Acceptor Molecular System, Int. J. Curr. Eng. Sci. Res. 4 (2014) 2342–2345.

[67] M. Homocianu, A. Airinei, Intra-/inter-molecular interactions - Identification and evaluation by optical spectral data in solution, J. Mol. Liq. 225 (2016) 869–876.

[68] R.S. Moog, D.D. Kim, J.J. Oberle, S.G. Ostrowski, Solvent Effects on Electronic Transitions of Highly Dipolar Dyes: A Comparison of Three Approaches, J. Phys. Chem. A 108 (2004) 9234–9301.

[69] Y. Li, T. Tan, S. Wang, Y. Xiao, X. Li, Highly solvatochromic fluorescence of anthraquinone dyes based on triphenylamines, Dyes Pigm. 44 (2017) 262–270.

[70] S.B. Katariya, D. Patil, L. Rhyman, I.A. Alswaidan, P. Ramasami, N. Sekar, Triphenylamine-based fluorescent NLO phores with ICT characteristics: Solvatochromic and theoretical study, J. Mol. Struct. 1150 (2017) 493–506.

[71] E. Stojanovska, C. Canbay, E.S. Pampal, M.D. Calisir, O. Agma, Y. Polat, R. Simsek, N.A.S. Gundogdu, Y. Akgul, A. Kilic, A review on non-electro nanofiber spinning techniques, RCS Adv. 6 (2016) 83783–83801.